Received: 1 September 2020 | Revised: 13 February 2021 | Accepted: 7 May 2021

DOI: 10.1002/eqe.3480

RESEARCH ARTICLE

WILEY

Nonlinear truss models for strain-based seismic evaluation of planar RC walls

Xianjue Deng[1] | **Ioannis Koutromanos**[2] | **Juan Murcia-Delso**[3] | **Marios Panagiotou**[4]

[1] Department of Civil, Architectural and Environmental Engineering, The University of Texas at Austin, Austin, Texas

[2] Department of Civil and Environmental Engineering, Virginia Polytechnic Institute and State University, Blacksburg, Virginia

[3] Department of Civil and Environmental Engineering, Polytechnic University of Catalonia (UPC-BarcelonaTech), Barcelona, Spain

[4] Nabih Youssef Structural Engineers, Los Angeles, California

Correspondence
Juan Murcia-Delso, Dept. of Civil and Environmental Engineering, Polytechnic University of Catalonia, C. Jordi Girona 1–3 (Building C1), Barcelona 08034, Spain.
Email: juan.murcia-delso@upc.edu

Abstract

This paper introduces a new approach for the seismic performance evaluation of planar RC walls. Compared to existing assessment guidelines, such as those in ASCE/SEI 41-17, where performance limits are described by plastic rotation or lateral drift, the proposed method uses local (strain) quantities, obtained from computational models. The analyses rely on a user-friendly implementation of the nonlinear truss model for RC structures, which eliminates the need to manually create a line-element representation of a wall and includes a material law for steel accounting for buckling and rupture of reinforcement. The capability of the models to capture common failure patterns for planar walls is validated for a set of six previously tested wall components which experienced a variety of damage modes (bar rupture, boundary element failure, diagonal compression and tension failures). The analytical models accurately predict the lateral strength, deformation capacity and failure modes observed in the tests. A set of acceptance criteria, based on the analytically obtained concrete and steel strains, is then established for the immediate occupancy, life safety and collapse prevention levels, consistent with different levels and types of damage. An initial calibration of the limit values associated with these criteria is proposed and verified using the analytical results for the six walls considered. The results of the proposed assessment methodology applied to the six walls are compared to those obtained using the nonlinear procedures in ASCE/SEI 41-17. The results indicate that ASCE/SEI 41-17 may not accurately describe the deformability of walls exhibiting mixed flexure-shear inelastic deformations.

KEYWORDS

acceptance criteria, computational model, performance level, performance-based assessment, reinforced concrete, structural walls

1 | INTRODUCTION

Reinforced concrete (RC) structural walls are a common structural system for buildings in many regions of high seismic hazard, such as the West Coast of the United States, New Zealand, or Chile. The seismic behavior of RC walls can be

governed by a variety of mechanisms and damage patterns, such as flexural and diagonal cracking, vertical bar buckling and rupture, and diagonal crushing of the wall web. A significant portion of RC wall buildings have been constructed prior to the implementation of modern seismic codes. The walls in these buildings may additionally be susceptible to horizontal sliding and lap-splice failures. The use of accurate and practical analytical procedures is deemed necessary to evaluate the seismic performance of existing RC wall buildings in earthquake-prone regions.

The ASCE/SEI 41–17[1] standard for seismic evaluation and retrofit of buildings defines target performance levels for different seismic hazard levels, together with modeling procedures and acceptance criteria to assess structural and nonstructural components. Three main performance levels (limit states) are considered for structural components, namely, immediate occupancy (IO), life safety (LS), and collapse prevention (CP). The nonlinear analysis procedures proposed in this standard represent the response of concrete members classified as deformation-controlled (ie, elements permitted to deform beyond yield) through idealized load-deformation curves. For RC walls, the deformations correspond to either the rotations of flexural hinges or the overall lateral displacements of the components. While the peak resistance in the load-deformation relation is defined based on principles of structural mechanics, most of the idealized curve parameters (eg, yield point, deformation at peak strength, residual strength) and deformation thresholds comprising the acceptance criteria have been empirically established from experimental data. Experimental evidence is also required to determine the unloading and reloading branches of the cyclic force-deformation curves for nonlinear dynamic analysis. Section 7.6 of ASCE/SEI 41-17 also allows the use of alternative modeling parameters and acceptance criteria derived based on data obtained from physical testing, following a peer-review process. While Section 7.3.3 of this same standard allows the use of an approved alternative analysis procedure, there are no specific guidelines for the acceptance criteria to be used with alternative analysis methods or for employing these methods to calibrate modeling parameters and acceptance deformation (hinge rotation or drift) limits.

The deformation parameters and threshold values provided in ASCE/SEI 41-17 may not be accurate for wall configurations which differ from those in the experimental tests used for developing the idealized curves. For instance, model parameters defined in this standard for shear-dominated walls, such as the yield point and the onset of lateral strength degradation, are based on limited test data.[2] Recently, Epackachi et al[3] proposed new deformation parameters for rectangular, barbell, and flanged shear-critical walls based on a database comprised of 240 wall tests. Still, the deformation parameters reported from the experimental database presented a large scatter with respect to the proposed values. The use of performance metrics based on local (material) responses can be regarded as a promising alternative to empirically derived values for plastic hinge rotation and drift ratio. The advantage of focusing on the local response lies to the fact that the failure of a structural component is driven by the inelastic behavior and damage of the constituent materials. Establishing, for example, limit strain values for the concrete and reinforcing steel would be expected to lead to performance threshold metrics that have a good predictive capability for the entire range of wall configurations encountered in engineering practice, as the stress-strain behavior of a given material is unique and independent of the structural component geometry.

Performance evaluation methods based on strain criteria have been previously proposed for the seismic design of flexure-dominated RC elements. Notable contributions in this regard have been made in the development of displacement-based seismic design methodologies.[4,5,6] Priestley and Calvi[5] proposed two strain-based performance levels (limit states) for the seismic design of RC bridge columns, namely, serviceability and damage control. For the serviceability limit state, the maximum compressive strain of concrete was limited to 0.4% and the tensile strain of vertical steel reinforcement to 1.5%. These thresholds were intended to limit concrete cracking and residual crack widths. For damage control, a concrete strain limit was established based on a conservative estimate of the ultimate compressive strain (corresponding to the fracture of hoops confining the column core), and the vertical steel strain was limited to 60% of its ultimate strain to avoid buckling and rupture. Local flexural demands were related to the global column response assuming the inelastic deformations were concentrated over an effective plastic hinge length. Recently, Kowalsky[7] proposed similar strain limits for RC columns for three performance levels, namely, fully operational, operational, and LS. The fully operational and operational levels are conceptually equivalent to the serviceability and damage-control limit states proposed by Priestley and Calvi.[5] The LS limit proposed by Kowalsky[7] corresponded to a concrete strain value 40% higher than the ultimate compressive strain proposed by Priestley and Calvi,[5] while the tensile strain limit for the reinforcing steel was equal to the strain corresponding to bar buckling. The displacement-based design method for RC walls by Panagiotou and Restrepo[8] set the acceptance limit for IO at 1% tensile strain for the vertical reinforcement and 0.4% compressive strain for the concrete, based on the assumption that these strain values would entail no visual damage for a wall. For the LS level, the same method established a limit tensile strain of 5% in the vertical reinforcement, to avoid premature steel fracture. Humar et al[9] limited the compressive strains of the unconfined and confined concrete in RC walls to 0.4% and 1.5%, respectively, to ensure a LS performance level.

The formulation and implementation of alternative performance assessment criteria based on strains or other quantities at the material level critically hinges on the use of a sufficiently accurate simulation scheme (constitutive laws, element formulations, etc), which will capture the salient aspects of material nonlinearity, and all the damage modes at the material level, which drive stiffness and strength degradation at the structural component level. A number of modeling approaches have been proposed to simulate the nonlinear behavior of RC walls. Beam-column models with a fiber-section law are commonly used for flexure-dominated RC members. One such analytical scheme by Pugh et al[10] was shown to be capable of capturing the strength degradation due to compressive toe crushing or bar rupture for a set of experimentally tested walls. It is worth mentioning that the reinforcing steel model used in the specific study included an ad hoc modification, which ensured that the material would fail when the tensile strain reached a threshold value, which was determined based on the instant at which bar rupture occurred in the wall test. Such an ad hoc approach cannot be used for predictive simulations, where the precise strain value for which rupture occurs will not be known beforehand. To model shear-dominated behavior in the context of beam-based models, several researchers have proposed combining biaxial concrete laws with a fiber section to account for flexure-shear interaction.[11] However, these models have not been shown to be capable of capturing diagonal shear failures. A few studies involving continuum finite element analysis with smeared-crack material models have been able to capture diagonal shear failures,[12] but the complexity and computational effort associated with such models make them unattractive for engineering practice and inappropriate for use in parametric analyses of building systems. A modeling scheme capable of predicting several aspects of the behavior of walls at a lower computational cost is the multiple-vertical linear element model (MVLEM), originally created by Massone et al[13] and further refined by Kolozvari et al.[14] In the MVLEM, a wall is represented by an assembly of RC panel elements, which develop normal and shear stresses, and are connected with rigid horizontal beam elements at the top and bottom of each wall element. The MVLEM has been shown capable of well capturing the axial-shear-flexure interaction in the prepeak regime of wall response, but it does not accurately capture strength degradation after the onset of shear or mixed flexure-shear failure. This limited capability to account for shear failures may be attributed to the existence of the rigid beam elements essentially enforcing a plane-section kinematic condition, which may not be a valid assumption after the development of significant inelastic deformations. Furthermore, the material law used for the reinforcing steel in the MVLEM cannot account for bar buckling and rupture, which is one of the main material damage modes driving lateral strength degradation and failure in wall components.

An alternative approach that has shown promise for the analysis of RC walls is the use of nonlinear truss models.[15,16] The key conceptual step in a truss model is the replacement of a wall member with an assemblage of line (truss) elements. Truss models are advantageous compared to the MVLEM, as they do not enforce a plane-section condition and consider biaxial behavior of concrete. The most recent modeling scheme of this type is the beam-truss model (BTM) by Lu et al[17] which allows the simulation of various types of wall geometries (eg, rectangular, nonplanar, etc) and other components such as coupling slabs. Additionally, the BTM has been shown to capture the axial-shear-flexure interaction, diagonal cracking and diagonal compressive failure, and strength degradation,[17,18] as well as out-of-plane plastic-hinge buckling.[19] Recently, truss models and the BTM have also been used to simulate the response of coupled structural walls, capturing the degradation and shear failures of the wall piers and coupling beams.[20,21] Despite the extensively validated accuracy of truss models, previous studies using the specific modeling approach did not explicitly account for certain inelastic mechanisms, such as bar buckling and rupture, which may be important for simulating damage and failure of walls.

The present study is aimed to contribute an alternative seismic evaluation procedure for planar RC walls, using computational simulation and acceptance criteria directly linked to material damage for the IO, LS, and CP performance levels. The simulation relies on a user-friendly implementation of the nonlinear truss model, which eliminates the need to manually define a line-element representation of a wall component. Another substantial enhancement in the employed analysis method, compared to previous work using truss models, is that the present study incorporates a material law for reinforcing steel that can capture the impact of bar buckling and rupture and can account for compressive crushing in confined boundary regions of walls. The modeling approach is validated with data from six experimental tests of wall components that had been previously tested and exhibited flexure, diagonal compression or diagonal tension failures. To the authors' knowledge, this is the first time that a modeling scheme of any type is shown to be capable of accurately capturing the global hysteretic response and failure modes of walls exhibiting such a range of damage patterns. To evaluate the seismic performance of walls using this modeling approach, alternative acceptance criteria, directly linked to damage in concrete and steel (eg, concrete cracking and crushing, steel rupture), are formulated in terms of strains and other strain-dependent material variables. A set of strain-based acceptance limits is proposed for use with truss models, and an initial calibration of the values associated with each criterion is proposed and validated using the analytical results for the six walls

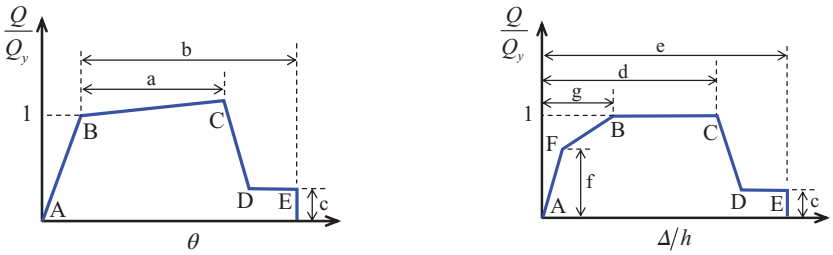

A) Flexure-dominated walls B) Shear-dominated walls

FIGURE 1 Force-deformation curves established in ASCE/SEI 41-17 for RC wall components (figures reproduced from ASCE/SEI 41–17[1])

considered. Finally, the results of the proposed strain-based performance evaluation of the wall specimens are compared to those obtained with the procedures established in ASCE/SEI 41-17.

2 | ASCE 41-17 EVALUATION PROCEDURES AND INELASTIC RESPONSE MODES FOR RC WALLS

Reinforced concrete wall components are classified in ASCE/SEI 41-17 as deformation-controlled or force-controlled, depending on their role in the lateral load resisting system (primary or secondary) and their ability to sustain inelastic deformations. Primary RC wall components exhibiting some level of deformation capacity beyond yield are generally considered as deformation-controlled. The response of deformation-controlled RC wall elements is classified in ASCE/SEI 41-17 as flexure- or shear-dominated. Evaluation procedures in this standard involving nonlinear static or dynamic analysis depend on establishing and using archetypical load-versus-deformation curves for the structural components, assuming that the response is deformation-controlled. These curves give the resistance Q, normalized by the corresponding yield value Q_y, as a function of the deformations. The latter are quantified by the plastic rotation θ and drift ratio Δ/h, for walls governed by flexure and shear, respectively. The normalized curves involved in this procedure are schematically presented in Figures 1A and B for walls dominated by flexure and shear, respectively. Detailed guidelines for obtaining the yield value Q_y, initial stiffness, and the other quantities listed in Figure 1 can be found in ASCE/SEI 41-17.

The FEMA 306 document,[22] to which the Commentary of ASCE/SEI 41-17 refers for further guidelines pertaining to evaluation of RC walls, distinguishes 12 different inelastic response modes. One mode corresponds to a ductile, flexure-dominated response, five modes correspond to brittle failures (boundary-zone compression, diagonal tension, diagonal compression, sliding shear, lap-splice failure) and six are combined (mixed) modes, characterized by intermediate ductility capacity (flexure/boundary-zone compression, flexure/diagonal tension, flexure/diagonal compression, flexure/sliding shear, flexure/lap-splice failure, flexure/out-of-plane wall buckling). In the mixed modes, the flexural strength of the wall initially governs the resistance, but strength degradation is ultimately triggered by a shear, buckling, or lap-splice failure mode. The present study will focus on RC walls exhibiting flexural, flexure/diagonal tension, and flexure/diagonal compression modes, which are the most common behavior types for isolated walls and walls with strong pier/weak spandrel configurations.[22] Behavior modes involving sliding shear, lap-splice failure, and out-of-plane wall buckling failures are not considered here. The typical evolution of damage for the three types of behavior considered herein is summarized as follows.

- Flexure: Walls dominated by flexure develop flexural cracks at relatively low lateral deformation levels. The ductility capacity of the walls is contributed by the tensile yielding of the vertical reinforcement. The lateral load capacity of the wall is generally attained when the concrete cover at the wall toe begins to crush due to large compressive strains. Walls with sufficient and well-detailed tie reinforcement in the boundary regions can undergo significant deformations beyond this point, and they may ultimately fail due to buckling and rupture of the vertical reinforcement (Figure 2A). Conversely, walls with poorly confined boundary elements will tend to experience bar buckling and crushing of the boundary zone at lower ductility levels.
- Flexure/diagonal tension: This type of behavior resembles that of flexure-dominated walls up to the point at which the flexural strength of the wall is achieved. While diagonal cracks may be more evident than for flexure-dominated walls at early stages of loading, the vertical reinforcement will yield and the wall will be able to develop its full flexural capacity. However, inelastic deformations reduce the shear capacity of the wall leading to a more brittle failure governed by the opening of one or more wide diagonal cracks, and eventually fracture of horizontal reinforcement (Figure 2B).

A) Vertical bar rupture in flexure-dominated wall (figure from Dazio et al.[23])

B) Diagonal tensile (shear) failure (figure from Lu et al.[24])

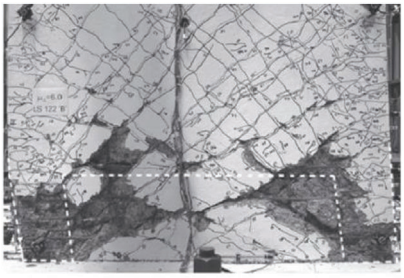

C) Crushing in wall web (figure from Beyer et al.[25])

FIGURE 2 Example of damage patterns occurring in RC walls during earthquake loading

- Flexure/diagonal compression: This type of behavior is typical of walls subjected to high shear forces but having sufficient strength against diagonal tension failure. The behavior of the wall is similar to the previous cases up to the point at which the flexural strength is achieved. After this point, diagonal cracks in the web become more prominent but cannot open widely due to the amount of horizontal steel and/or the restraint provided by stiff boundary elements or wall flanges. Strength degradation is eventually caused by the spalling of concrete between diagonal cracks in the web (Figure 2C), that is, by the failure of the diagonal compressive strut enabling the shear-resisting mechanism.

3 | DESCRIPTION OF MODELING SCHEME FOR PERFORMANCE ASSESSMENT

This section describes the modeling scheme to be used for the performance evaluation of RC walls. The element formulation is described first, followed with a discussion of the employed constitutive models for concrete and reinforcing steel.

3.1 | Element formulation

The adopted analysis method constitutes a user-friendly implementation of the nonlinear truss model in the program *FE-MultiPhys*.[26] The truss model substitutes a wall component with an assemblage of horizontal, vertical and inclined (diagonal) line elements, as shown in Figure 3A. The present study is focused on two-dimensional analysis of essentially planar walls, at which case the line elements can use a two-dimensional truss formulation. The specific approach is well suited for parametric analysis of RC components and systems, as it essentially relies on uniaxial stress-strain laws and is characterized by numerical efficiency compared to, for example, continuum-based finite element models. The only potential limitation of the method is the need to manually define the truss representation of a RC component, which may be cumbersome for practitioners and researchers. To address this potential issue, the present analysis approach is implemented in such a fashion that each truss standard panel—consisting of four nodes in a rectangular arrangement connected through two horizontal, two vertical and two diagonal truss elements—is programmed as a rectangular, four-node macroelement, as schematically summarized in Figure 3B. While the truss panel is represented as a rectangular element, facilitating the model definition and the postprocessing of the results, the actual computations for the set of four nodes comprising the panel (ie, the calculation of internal nodal force vector and tangent stiffness matrix for the specific nodes) use an underlying truss panel assemblage, which is "hidden" from the user. In this way, the accuracy and efficiency of the truss model become easily available to users, while also eliminating the need to manually create an assemblage of line elements to represent a wall. A similar approach has been previously used by Zhang et al[27] for postprocessing the results of analyses based on truss models. Contrary to that earlier work, the present study employs a generic implementation of a rectangular macroelement, which affects all stages of a computational simulation (preprocessing, analysis, and postprocessing).

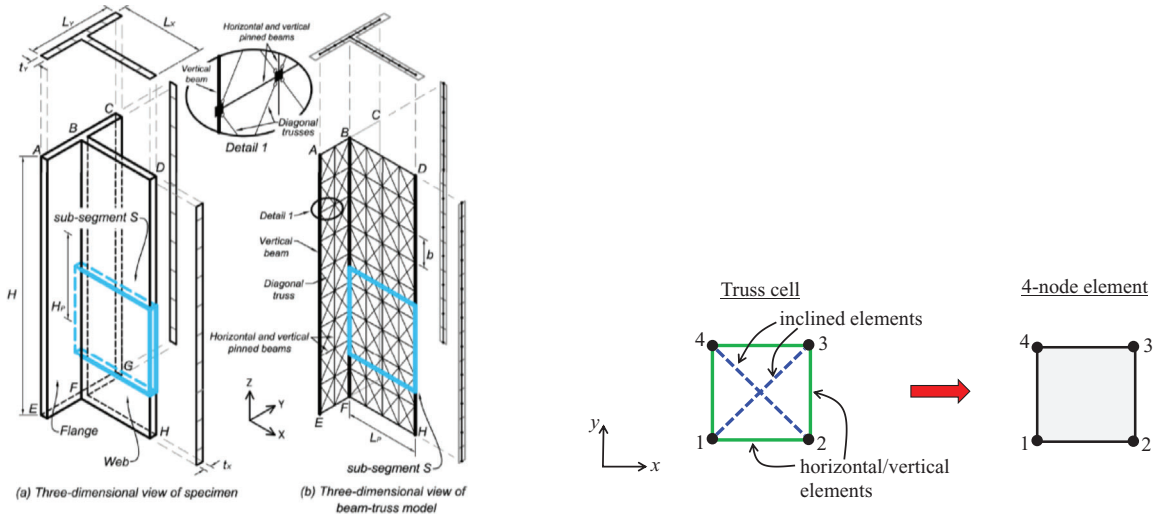

A) Representation of RC wall as assemblage of line elements (figure from Lu et al.[17])

B) Formulation of a truss standard panel assemblage as a rectangular, four-node macro-element

FIGURE 3 Schematic summary of user-friendly implementation of the truss model

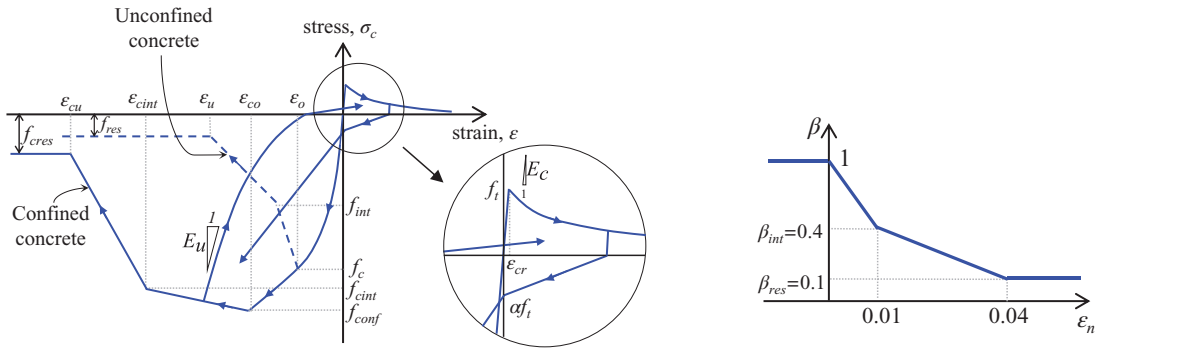

A) Monotonic and cyclic hysteretic responses

B) Reduction of compressive stress in inclined truss elements due to transverse tensile strain

FIGURE 4 Behavior of material model for concrete

3.2 | Constitutive models for concrete and reinforcing steel

The uniaxial constitutive law for concrete, which is schematically summarized in Figure 4A, has been originally formulated by Lu and Panagiotou.[28] The specific material model can account for the strength and stiffness degradation associated with tensile cracking and compressive crushing. It can also account for the increased compressive strength and deformability of confined concrete. As shown in Figure 4A, compressive strength degradation for unconfined and confined concrete occurs when the magnitude of the strain exceeds a threshold value equal to ε_o and ε_{co}, respectively. After this point, the concrete exhibits linear softening, until it reaches a strain value equal to ε_u and ε_{cu}, respectively, for unconfined and confined concrete. Softening in the postcrack tensile strain regime is described by an exponential curve. For the diagonal truss elements, the concrete constitutive law accounts for the effect of transverse tensile strains on the compressive resistance, in accordance with the work of Vecchio and Collins.[29] Specifically, compressive axial stresses for the truss elements are multiplied by a reduction coefficient, β, which expresses the effect of transverse tension on the compressive stress of concrete. The value of β depends on the transverse tensile strain of each truss element in accordance with the law presented in Figure 4B. Since the stress-strain relations schematically shown in Figure 4 include softening, it is necessary to ensure that the analysis scheme is not affected with spurious mesh-size effects associated with localization. This is accomplished through use of the regularization scheme presented in Lu and Panagiotou,[28] which is based on the stipulation that the stress-strain laws defined for the material of the truss elements correspond to an element whose length is equal to a reference length value, L_{ref}.

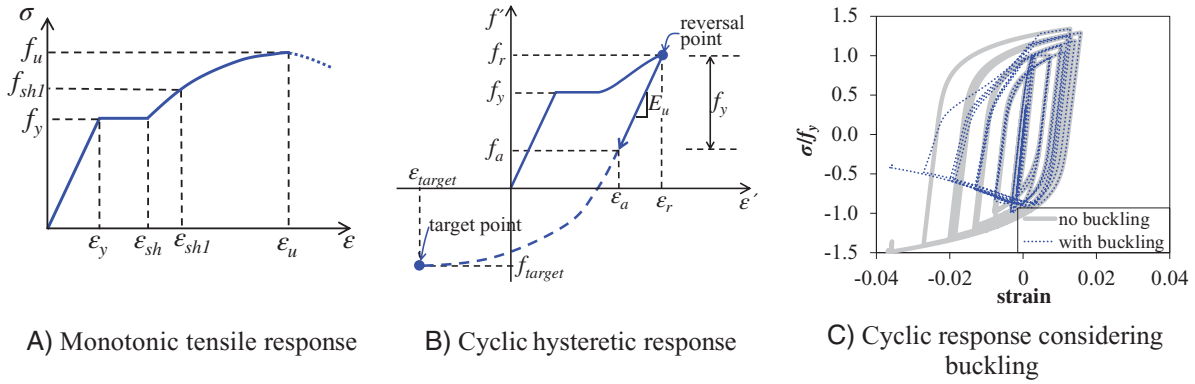

A) Monotonic tensile response B) Cyclic hysteretic response C) Cyclic response considering buckling

FIGURE 5 Behavior of material model for reinforcing steel (figures from Girgin et al)[33]

Previous studies using nonlinear truss models[17–21] used material laws for the reinforcing steel which were not accounting for the effect of buckling and for material failure (rupture) due to cyclic inelastic loading. To provide the truss models with the capability to account for bar buckling and rupture, the present study uses the uniaxial constitutive law recently proposed by Kim and Koutromanos.[30] This law represents the hysteretic stress-strain behavior using the equations previously proposed by Dodd and Restrepo[31] and a noniterative stress-update algorithm. It has been successfully used in simulations involving both refined finite element models[32] and simplified, beam-based models.[33] In the absence of buckling or rupture, the material model can be fully calibrated if the stress-strain curve in monotonic tension, schematically shown in Figure 5A, is known. The constitutive model includes a hysteretic law to capture the cyclic response of reinforcing steel, as qualitatively shown in Figure 5B. Buckling is modeled using a criterion defined in terms of axial stress, proposed in Kim and Koutromanos.[30] This criterion was derived analytically for a bar segment of length L, assuming that buckling occurs when the increment dN in axial force corresponding to a reference axial strain increment is equal to zero, due to the spontaneous occurrence of a curvature associated with the transverse deflection of the bar segment. After the buckling criterion is met, the stresses obtained for compressive strains beyond the strain at onset of buckling are multiplied by a reduction factor. A schematic comparison of hysteretic stress-strain response adjusted for buckling, as compared to the hysteretic response in the absence of buckling, is provided in Figure 5C. The buckling criterion and the law to account for the buckling effect on the axial stress require the calibration of an additional slenderness parameter, L/d, defined as the ratio of the bar segment that buckles over the diameter d of the bar. For reinforced concrete members, the value of L/d can be defined using a procedure proposed by Dhakal and Maekawa[34] and shown by Girgin et al[33] to be capable of accurately describing the occurrence of buckling in RC members subjected to cyclic loads. The bar rupture under cyclic strain histories is accounted for through a criterion based on the accumulation of a quantity D. Specifically, given the true material stress, f, and the plastic strain rate, $\dot{\varepsilon}_p$, the evolution of D is governed by the following rate equation.

$$\dot{D} = \begin{cases} \left(\frac{f}{f_y}\right)^{2t} \dot{\varepsilon}_p, & if\, f > 0 \\ 0 & otherwise, \end{cases} \tag{1}$$

where f_y is the yield stress and t is a material constant. Material failure, that is, rupture, occurs when the value of D becomes equal to D_{cr}, which is also a parameter of the material model. Once the rupture criterion is met at a location of a structure, the material model is rendered incapable of developing any resistance for the remainder of the loading process.

4 | ANALYSIS OF WALL COMPONENTS UNDER CYCLIC LOAD

The modeling scheme described in the previous section is used for the analysis of six RC wall specimens, which have been experimentally tested in the past by different research groups. Information for each wall is summarized in Table 1. Since the analyses are meant to allow a preliminary validation of strain-based performance metrics, the selection of the wall specimens needs to include a variety of failure mechanisms. Three specimens exhibited a flexure-dominated damage pattern. Strength degradation was caused by reinforcing steel rupture in two of these specimens, and by boundary concrete

TABLE 1 Summary of walls considered in analytical study

Wall ID	Reference	Failure mode	θ_d (°)	a (mm)	Wall length to element size ratio	Boundary element to length ratio	ρ_b(%)	$\rho_{w,v}$(%)	$\rho_{w,h}$(%)	Axial load ratio (%)
Wall #1	Dazio et al[23]	Boundary crushing	57.0	162.5	12	0.16	1.54	0.54	0.25	10.8
Wall #2	Dazio et al[23]	Boundary vertical bar fracture	51.3	100.0	20	0.10	1.54	0.54	0.25	5.8
Wall #3	Segura and Wallace[38]	Boundary vertical bar fracture	45.0	152.4	15	0.13	3.68	0.37	0.49	7.5
Wall #4	Tran and Wallace[39]	Diagonal tension, boundary crushing	58.0	75.0	16	0.12	3.33	0.27	0.27	10.0
Wall #5	Mestyanek[40]	Diagonal tension	45.0	138.9	18	0.06	3.01	0.16	0.16	0
Wall #6	Oesterle et al[41]	Web crushing	56.7	152.5	12	0.16	3.67	0.29	0.63	13.4

Note: θ_d is angle between diagonal truss elements and the horizontal direction, a is horizontal length of macroshell, ρ_b is the boundary vertical reinforcement ratio, $\rho_{w,v}$ is the web vertical reinforcement ratio, $\rho_{w,h}$ is the web horizontal reinforcement ratio.

TABLE 2 Material model parameters for unconfined concrete

Wall ID	f_c (MPa)	ε_o	f_{int} (MPa)	ε_{int}	f_{res} (MPa)	ε_u	f_t (MPa)	M
Wall #1	45.6	0.002	12.0	0.004	5.0	0.007	2.23	0.050
Wall #2	39.2	0.002	12.0	0.004	5.0	0.008	1.07	0.050
Wall #3	46.3	0.002	12.0	0.004	5.0	0.007	2.25	0.039
Wall #4	47.1	0.002	12.0	0.004	5.0	0.007	2.26	0.034
Wall #5	27.0	0.002	12.0	0.004	5.0	0.009	1.71	0.020
Wall #6	21.8	0.002	12.0	0.004	5.0	0.010	3.00	0.036

Note: f_c is the concrete compressive strength, ε_o is the strain at peak compressive strength, f_{int} and ε_{int} are the stress and strain values corresponding to an intermediate point for the postpeak compressive softening regime, f_{res} is the residual compressive strength, ε_u is the strain magnitude where residual strength is reached, f_t is the concrete tensile strength, M is the ratio of residual tensile strength over tensile strength for vertical elements, accounting for tension-stiffening effect, based on equation from Lu et al.[24]

crushing in the other one. Two of the remaining specimens initially presented a flexure-dominated behavior but incurred a diagonal tension failure. Specifically, one specimen failed through the simultaneous occurrence of a large diagonal crack and boundary concrete crushing, and the other failed through the formation of a major diagonal crack. The sixth and final specimen exhibited a flexure/diagonal compression behavior. For relatively low levels of lateral displacement, this wall specimen had a flexure-dominated response, until the occurrence of significant strength degradation due to web crushing.

The dimensions of the rectangular macroelements used in the discretization of each wall are obtained as follows. First, the in-plane inclination angle, θ_d, of the truss elements in a truss panel is defined, using the expression proposed in Lu et al.[17] The dimension a of the rectangular elements parallel to the length of the wall is established next, based on the desired level of discretization. To balance accuracy and computational effort, the size of a has been so determined to have one or two elements for each boundary region. This results in wall length-to-element ratios between 12 and 20, as shown in Table 1. Finally, the element dimension parallel to the height of the wall is set equal to $a \bullet \tan\theta_d$.

The material parameters for the unconfined concrete, confined concrete and reinforcing steel are assigned the values presented in Tables 2, 3, and 4, respectively. Confined concrete behavior is assumed to characterize only the compressive response of the vertical elements located in the confined boundary regions of each wall. The compressive strength of the concrete has been determined based on material test data reported in the experimental studies. All other parameters of the concrete constitutive law are calibrated based on equations proposed by Mander et al[35] and Karthik and Mander.[36] For unconfined concrete, the reference length value, L_{ref}, is set equal to 600 mm for the horizontal and vertical truss elements, and equal to 850 mm for the inclined elements. The specific values of L_{ref} were established by Lu and Panagiotou,[28] based on the length of the sides and diagonals of the unconfined concrete panels used in the study by Vecchio and Collins.[29]

TABLE 3 Material model parameters for confined concrete

Wall ID	f_{cc} (MPa)	ε_{co}	f_{cint} (MPa)	ε_{cint}	f_{cres} (MPa)	ε_{cu}	f_t (MPa)	M
Wall #1	54.1	0.004	20.5	0.021	5.0	0.025	2.23	0.096
Wall #2	48.2	0.004	21.0	0.022	5.0	0.026	1.07	0.096
Wall #3	73.0	0.008	38.7	0.042	5.0	0.046	2.25	0.158
Wall #4	61.6	0.006	26.5	0.028	5.0	0.032	2.26	0.200
Wall #5	29.4	0.003	14.4	0.014	5.0	0.018	1.71	0.190
Wall #6	28.9	0.005	19.1	0.024	5.0	0.028	3.00	0.144

Note: f_{cc} is increased concrete compressive strength due to confinement, ε_{co} is the strain at peak confined compressive strength, f_{cint} and ε_{cint} are the stress and strain values corresponding to an intermediate point for the postpeak compressive softening regime, f_{cres} is the residual compressive strength, ε_{cu} is the strain magnitude corresponding to complete compressive strength degradation to the residual value f_{cres}.

TABLE 4 Material model parameters for steel reinforcement

Wall ID	Bar Size (mm)	E_s (MPa)	f_y (MPa)	ε_{sh}	ε_{sh1}	f_{sh1} (MPa)	ε_u	f_u (MPa)	L/d	D_{cr}
Wall #1	6	200,000	519	0.003	0.04	545	0.055	559	N/A	0.13
	8	200,000	584	0.003	0.04	690	0.079	714	18.75	0.13
	12	200,000	576	0.003	0.04	640	0.073	675	4.17	0.16
Wall #2	6	200,000	489	0.003	0.04	530	0.065	552	N/A	0.13
	8	200,000	569	0.003	0.04	650	0.073	700	18.75	0.13
	12	200,000	601	0.003	0.04	680	0.077	726	6.25	0.15
Wall #3	8	200,000	439	0.016	0.04	500	0.071	531	N/A	0.14
	9.5	200,000	454	0.012	0.04	680	0.124	706	16.0	0.39
	16	200,000	489	0.012	0.04	630	0.143	669	3.2	0.22
Wall #4	6	200,000	450	0.003	0.04	550	0.109	661	23.33	0.23
	6	200,000	516	0.003	0.04	530	0.060	580	N/A	0.03
	12.7	200,000	472	0.013	0.04	600	0.109	620	3.94	0.23
Wall #5	6	190,000	472	0.014	0.03	550	0.200	658	N/A	0.38
	12	193,000	451	0.018	0.03	500	0.290	608	5.83	0.55
Wall #6	3	200,000	487	0.015	0.04	500	0.109	510	N/A	0.15
	6	200,000	512	0.015	0.04	630	0.080	676	16.0	0.14
	19.1	200,000	441	0.007	0.04	620	0.109	733	1.78	0.25

Note: E_s is Young's modulus, f_y is bar yield stress, ε_{sh} is strain at onset of strain hardening, ε_{sh1} and f_{sh1} are the strain and stress of an intermediate point on hardening regime of the monotonic curve, f_u is ultimate strength, and ε_u is the strain corresponding to the ultimate strength. For steel used as horizontal reinforcement, no L/d value is defined, as buckling is not considered.

For confined concrete, the value of L_{ref} is set equal to 450 mm in the present study, as this was the gage length used to compute strains in the concrete cylinders tested in the work of Mander et al.[35] Several of the studies provided full stress-strain curve data for the reinforcing steel bars, obtained from monotonic tensile tests, which allowed the full calibration of the steel model parameters. The remaining studies only provided the yield and ultimate strength of the bars, at which case the other parameters of the steel model are assigned typical values previously used in the literature for the same grade of steel.

An incremental-iterative static scheme is used for the solution of the global equations of equilibrium in the models. The analyses use a geometrically linear description of deformations, since the only significant source of geometric nonlinearity for the cases considered would be attributed to buckling of the vertical reinforcing steel. As explained in the previous section, the bar buckling is accounted for phenomenologically at the stress-strain level of the material model for the reinforcing steel.

Preliminary analyses using the proposed modeling scheme indicated a potential issue for cases involving concrete crushing in the confined boundary regions of wall components. In such cases, it was observed that the overlap of inclined and vertical elements in these regions could lead to a spurious increase of the compressive resistance, which could prevent capturing the strength degradation associated with such type of failure. To address this potential issue, concrete failure is

enforced in all the elements comprising the 4-node macroshell whenever the strain of any vertical truss element reaches the compressive strain of confined concrete corresponding to the fracture of transverse reinforcement, ε_{cf}. The value of ε_{cf} is calculated using the energy balance method for the critical cross-tie proposed by Mander.[37] For Wall #1, which is the only specimen considered exhibiting softening in confined concrete in the analysis, ε_{cf} is equal to 0.013. Completely eliminating material resistance upon occurrence of crushing of confined concrete precludes spurious compressive forces due to overlap of multiple truss elements, and ensures that the wall strength degradation associated with crushing in confined boundary regions is properly captured.

Before proceeding with a presentation and discussion of the analysis results, a brief description of the main experimental observations from the tests of the walls considered is deemed necessary.

4.1 | Description of walls

Walls #1 and #2 considered herein are specimens WSH6 and WSH3, respectively, tested by Dazio et al.[23] Both walls were 4950 mm tall and had a rectangular cross-section with a length of 2000 mm and a thickness of 150 mm. A lateral load was applied at a height of 4560 mm and 4520 mm above the base, respectively. The confined boundary regions of the two walls had a length equal to 343 mm and 218 mm, respectively. A constant axial load was applied to both walls, which exhibited a ductile, flexure-dominated response. For Wall #1, strength degradation occurred due to rupture of transverse reinforcement and crushing of the core concrete in the boundary regions. Excessive buckling of the vertical reinforcement, without any rupture, was also observed. Wall #2 incurred strength degradation due to buckling and subsequent rupture of boundary vertical reinforcement.

Wall #3 corresponds to specimen WP6 tested by Segura and Wallace,[38] which had a height of 2134 mm and a rectangular cross-section with a length of 2286 mm and a thickness of 190.5 mm. The lateral loading was applied at the top of the specimen, which represents the bottom stories of an eight-story wall with a total height of 8170 mm. The boundary regions at the ends of the section had a length of 355 mm and included a large amount of reinforcement. A constant axial load and an overturning moment, aimed to simulate the seismic effect from higher floors, were applied on top of the specimen. The wall response was flexure-dominated. Wall deformation was reported as wall rotation in the assumed plastic hinge region corresponding to half of the wall length. The first vertical bar rupture occurred during the second cycle targeting a hinge rotation level of 2%, and did not entail any significant strength degradation. Strength degradation was observed during a loading cycle at a hinge rotation level of 3% and was caused by the occurrence of rupture in multiple vertical bars.

Wall #4 is specimen RW-A20-P10-S38 tested by Tran and Wallace,[39] having a rectangular cross-section 1220 mm long and 152 mm thick. The lateral load was applied at a height of 2440 mm above the wall-to-foundation interface, while the axial load was applied on top of the specimen. The confined boundary elements had a length of 178 mm. At early loading stages, the wall exhibited a hysteretic response which corresponded to a ductile, flexure-dominated mode. However, major shear cracks were noticed before the first yielding and evolved during the test procedure. Strength degradation was finally obtained at a drift ratio of 3% due to diagonal-tension failure, manifested through the simultaneous occurrence of a large inclined crack, fracture of web horizontal bars, and crushing of concrete at the toe of the wall.

Wall #5 corresponds to Unit 1.0 tested by Mestyanek.[40] This barbell-section wall had a height of 2500 mm and a length of 2500 mm. Lateral loading was applied at the top of the wall. On both sides of the cross-section, there were enlarged boundary columns with a length of 150 mm and a thickness of 200 mm. The wall web had a thickness of 100 mm and a length of 2200 mm. No axial load was applied to the wall. A diagonal-tension failure, manifested through the formation of a major diagonal crack, was obtained at a drift ratio of 1.11%. The ensuing strength degradation was attributed to the separation of the specimen into two wall segments which essentially deformed independently of one another for the remainder of the test. Concrete crushing and reinforcement buckling were also obtained in the boundary region of the wall. The boundary damage was attributed to the deformation of the individual wall segments after the formation of the diagonal crack and did not directly cause any lateral strength degradation.

Wall #6 is specimen B6 tested by Oesterle et al,[41] having a height of 4570 mm and a barbell cross-sectional shape, with two square end columns with a sectional dimension of 305 mm. The lateral load was applied at the top of the wall, which had a length of 1910 mm and a web with a thickness of 102 mm. Most of the horizontal and vertical reinforcement was concentrated at the two end columns. The specific wall had the highest axial load ratio among all cases considered in the present study. While the specimen initially exhibited a ductile, flexure-dominated response, it ultimately incurred significant strength degradation due to web crushing, first noticed at a drift ratio of about 1.1%. Significant strength degradation was not obtained until the occurrence of extensive crushing at a drift ratio of 1.7%.

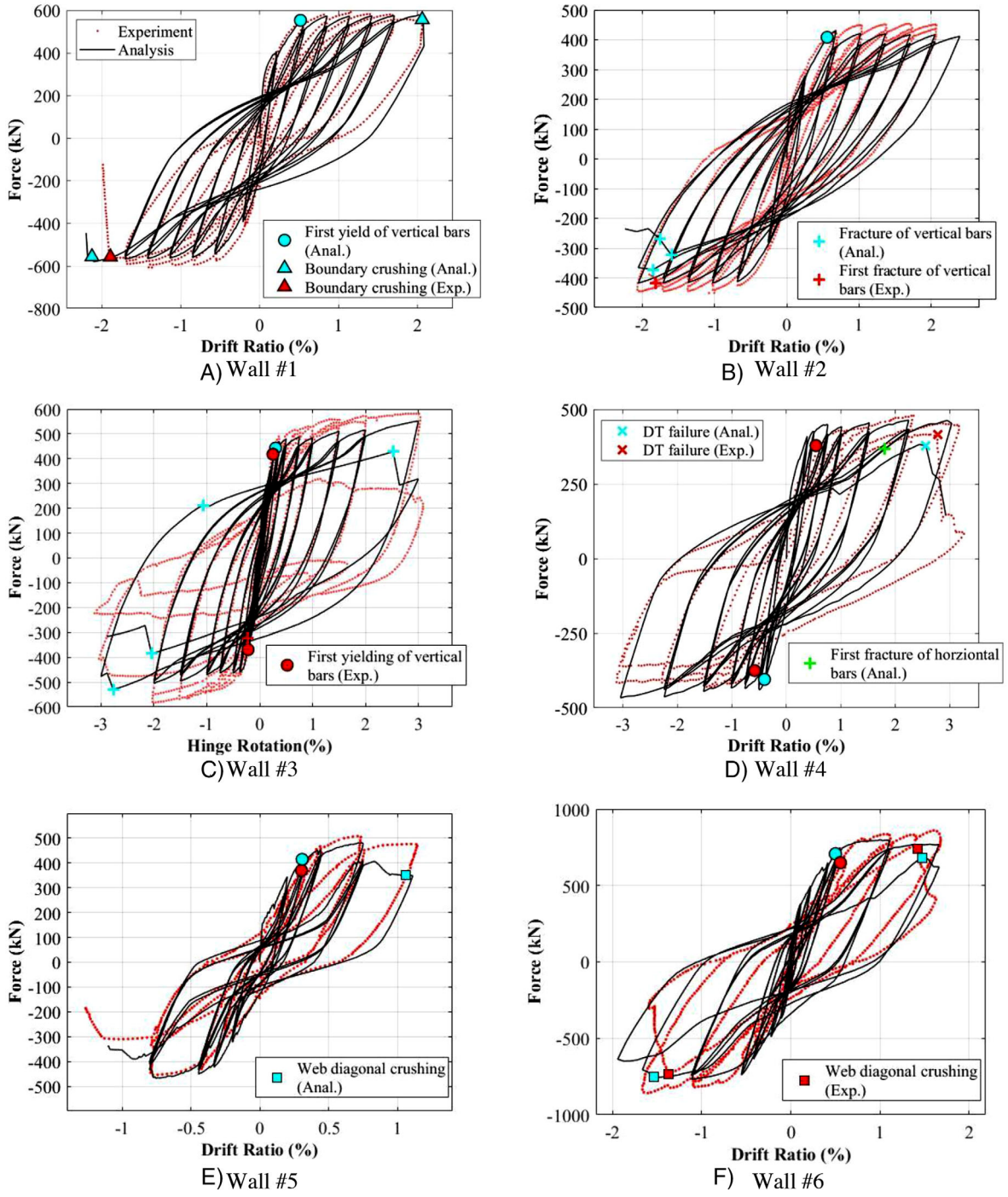

FIGURE 6 Comparison of analytical and experimental hysteretic curves of wall specimens with main damage events specified

4.2 | Analysis results

The analytically obtained lateral force-displacement curves for the walls are compared to the corresponding experimental curves in Figure 6. For Wall #3, the results are presented in terms of lateral force versus rotation of the assumed plastic hinge region to allow a direct comparison with the reported experimental results. Figure 7 compares the maximum principal strain contour plot at the end of each analysis to the damage pattern obtained at the end of the corresponding experimental test. A discussion of the principal observations from the analyses is provided for each of the walls.

The analytical results for Wall #1 are in good agreement with the experiment in terms of lateral strength, force-displacement envelope curve, and deformation level at which strength degradation occurred, as shown in Figure 6A.

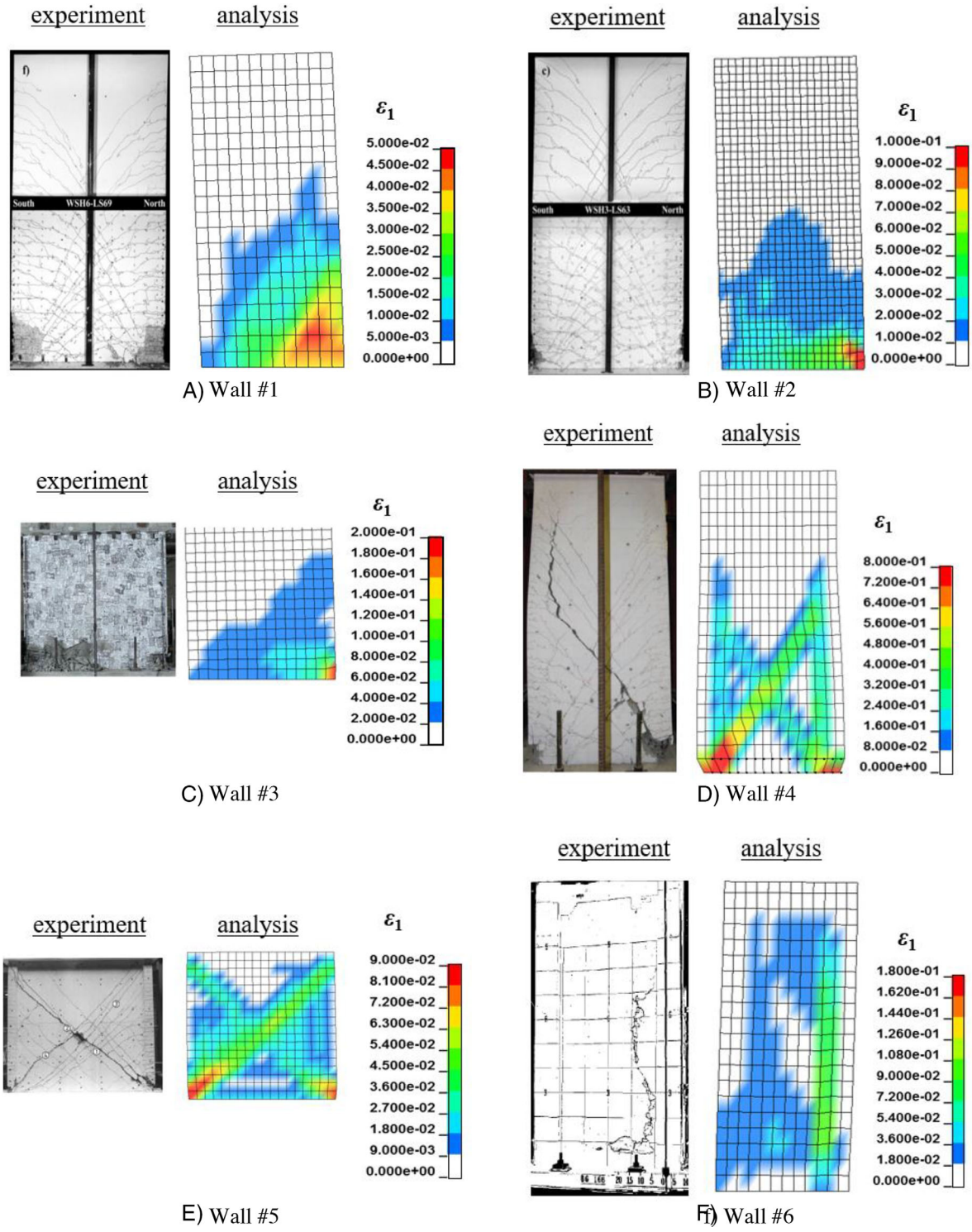

FIGURE 7 Comparison of experimentally observed damage patterns and maximum principal strain contour at the end of the analysis of the six walls considered in the analytical study

The analytically obtained hysteretic curves correspond to slightly higher energy dissipation than in the actual experimental test. As shown in Figure 7A, the contour plot of the maximum principal strains at the end of the analysis, where the model is subjected to a negative lateral displacement, indicates the occurrence of significant tensile strains over a band near the base, extending diagonally from the left bottom corner towards the opposite boundary. This pattern is consistent with flexural cracks extending diagonally through the web obtained in the test, as shown in Figure 7A. The vertical reinforcement in the model first yields at a drift ratio of 0.52%, while the point at which steel yielded was not reported in the

experiment. The analytical model predicts crushing of the concrete core in the boundary, triggering concrete failure in the entire shell element and significant strength degradation, in the positive and negative direction at drift levels of 2.05% and −2.12%, respectively. These values are very close to the experimental value of the drift at failure (−1.93%).

For Wall #2, the analytical results are consistent with the experiment in terms of lateral strength, hysteretic curve shape, ductility capacity, and drift level at occurrence of strength degradation due to vertical bar rupture, as shown in Figure 6B. The test was terminated when one of the vertical bars in the boundary region ruptured and the strength drop was less than 20%. To obtain a more severe damage stage for performance assessment purposes, the analysis considers one additional loading cycle, up to a drift ratio of 2.4%. The maximum principal strain distribution presented in Figure 7B has good correlation with the experimental cracking pattern and indicates a flexure-dominated response. The large tensile strain values obtained at the right side of the wall near the base are related to the occurrence of rupture of vertical reinforcing steel. First yielding of vertical reinforcement in the analysis is obtained at a drift ratio of 0.56%. The analytical model predicts first rupture of vertical steel during the second loading cycle at a drift ratio of 2%, which matches the instant of first fracture occurrence in the experiment. The additional loading cycle considered in the analysis leads to rupture of two more vertical bars. The rupture of several bars in the analysis lead to small and sudden drops to the value of lateral resistance, as deduced from Figure 6B.

The analytical results obtained for Wall #3 agree well with the experiment in terms of hysteretic curve shape, ductility capacity, onset of first yielding, and deformation level at occurrence of bar rupture, as shown in Figure 6C. The maximum principal strain contour obtained from the model is similar to that of Walls #1 and #2, and resembles the concrete crack pattern observed in the experiment, as shown in Figure 7C. The model predicts first yielding of vertical reinforcement at a hinge rotation of 0.29%, which agrees with the experimental observations (0.25% and 0.22%, for loading in the positive and negative directions, respectively). Rupture of vertical reinforcement occurs in the analysis at the loading cycle corresponding to a hinge rotation of 3%, which coincides with most of the bar fractures in the experimental test. It is worth mentioning that one vertical bar at the corner of the section ruptured during the last cycle at 2% rotation during the test, but this rupture did not lead to a noticeable strength degradation.

For Wall #4, the analytical model satisfactorily reproduces the lateral strength, hysteretic response, and deformation level at the onset of strength degradation, as shown in Figure 6D. It additionally reproduces the damage and failure patterns observed in the test. Specifically, the principal strain contour indicates the formation of two crossing diagonal bands of large tensile strains, as shown in Figure 7D, indicating the occurrence of large inclined cracks. The formation of the diagonal crack is accompanied by crushing at the boundary region of the wall. Rupture of multiple horizontal bars also occurs along the web-to-boundary interface, where large tensile strains are obtained. First yielding of vertical reinforcement is obtained at a drift ratio of −0.40%, while yielding in the test was first obtained at a drift level of ±0.55%. Strength degradation in the analysis occurs at a drift ratio of 2.68%, which is practically identical to the corresponding drift value (2.78%) in the experiment. It should be noted that, prior to the main strength degradation due to failure, small drops in the lateral resistance are observed in the analysis due to rupture of multiple horizontal bars. The first horizontal bar rupture is obtained at a drift ratio of 1.80%.

The analytical results obtained for Wall #5 provide a satisfactory prediction of the lateral strength, hysteretic curve shape, first yielding drift, and the drift ratio in which strength degradation occurs, as illustrated in Figure 6E. The maximum principal strain contour plot in Figure 7E indicates the formation of two major diagonal cracks, which is consistent with the type of damage observed in experiment. The model predicts first yielding at a drift ratio of 0.31%, while yielding in the test was first observed at a drift ratio of 0.30%. The model successfully reproduces the strength degradation at a drift level of 1.1%, caused by the degradation of the compressive resistance of the inclined truss elements due to the effect of transverse tension.

The analysis of Wall #6 is in good agreement with the experimental observations in terms of the hysteretic force-deformation curve, first yielding, and onset of strength degradation, as deduced from Figure 6F. Starting at a drift level of approximately 0.4%, the model presents bands of large tensile strains along the web-to-boundary interface. The shape of the hysteretic curves in the model corresponds to a slightly lower inelastic energy dissipation than that obtained in the experimental test. The behavior in the analysis is flexure-dominated until the occurrence of a diagonal compression failure, manifested as softening in the diagonal truss elements in the web of the wall, and leading to significant strength degradation. The web crushing also created a vertical failure plane around the web-to-boundary interface, which is consistent with the experiment observation of failure. First yielding of longitudinal steel is predicted at a drift ratio of 0.50%, which is close to the corresponding experimentally recorded value of 0.56%. The onset of softening in a diagonal truss element is used to determine the instant at which web crushing occurs. Web crushing is obtained at drift ratios of 1.48% and 1.53%, for loading in the positive and negative direction, respectively. These drift values are very close to the values

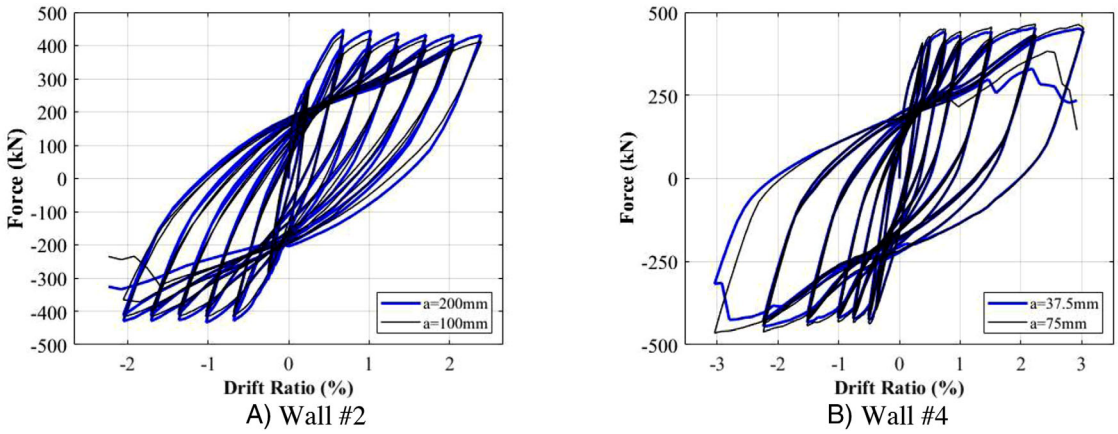

FIGURE 8 Comparison of results for different mesh sizes

corresponding to diagonal compression failure in the experimental test (1.42% for positive direction and 1.37% for negative direction).

To verify that the analytically obtained solutions do not have significant discretization errors and that the employed regularization approach adequately prevents spurious mesh-size effects associated with strain localization, the analyses for Walls #2 and #4 are repeated for a different element size parameter a. The analyses for Walls #2 and #4 are repeated for $a = 200$ mm and $a = 37.5$ mm, respectively. The value θ_d of the angle for the inclined truss elements is the same as the one provided in Table 1. The comparison of the load-displacement curves obtained for different values of mesh size is provided in Figures 8A and 8B, for Walls #2 and #4, respectively. It can be seen that the load-displacement curves obtained for each wall for two different values of mesh size are very similar. The same applies for the displacement at which strength degradation occurs and for the obtained damage pattern and failure mode.

5 | STRAIN-BASED PERFORMANCE ACCEPTANCE CRITERIA

This section establishes alternative performance evaluation criteria for RC walls, based on material strain or strain-dependent quantities obtained from analysis with truss models. A set of strain-based acceptance thresholds are provided for the IO, LS and CP performance levels in accordance with the definitions in the ASCE/SEI 41-17 document. As mentioned earlier, the use of performance metrics at the material level is considered to be advantageous because they are more directly linked to physical damage mechanisms (eg, cracking or crushing of concrete, bar rupture), and the material behavior and local damage modes are independent of wall configuration or behavior mode. Thus, there is no need for prior determination of the dominant behavior mode of the wall, and mixed flexure/shear modes can be naturally accounted for in the assessment. The acceptance criteria will be separately presented for each of the three performance levels.

5.1 | Immediate occupancy (IO) level

As defined in the ASCE/SEI 41-17 standard, the IO performance level corresponds to a condition at which no permanent damage has occurred, and the structure essentially retains the same strength and stiffness as in the preearthquake state. For wall components, this standard allows small levels of inelasticity for IO based on the prescribed limits of acceptable deformation. For flexure-dominated walls, irreversible damage may occur in the form of flexural (horizontal) crack opening or initiation of cover spalling in compression. Priestley et al[6] established a 1% strain in the vertical steel as an IO threshold, based on the expectation that steel strains lower than this value will limit residual crack widths to values between 0.5 and 1 mm. Panagiotou and Restrepo[8] used the same vertical steel strain value as the threshold for the IO level, as the limit for precluding the occurrence of visible damage in the wall.

Consistent with the ASCE/SEI 41-17 definitions and previous strain limits proposed for IO performance, the present study will also adopt a tensile strain of 1% in the steel as one of the limits for IO acceptance. Regarding cover spalling, irreversible damage is assumed to occur when the vertical elements at either end of the wall section reach a compressive

TABLE 5 Proposed strain-based acceptance criteria for different performance states

Performance level	Damage modes to be prevented	Strain-based acceptance criteria
IO	Large flexural cracks	$\varepsilon_s \leq 1.0\%$
	Large inclined (shear) cracks	$\varepsilon_{c,diag} \leq w_{cr}/L_d$
	Concrete cover spalling	$\lvert\varepsilon_{c,vert}\rvert \leq \lvert\varepsilon_0\rvert$
LS	First fracture of vertical or horizontal steel	$D \leq D_{cr}$
	Onset of confined concrete crushing	$\lvert\varepsilon_{c,vert}\rvert \leq 0.75\lvert\varepsilon_{cf}\rvert$
	Onset of web concrete crushing	$\lvert\varepsilon_{c,diag}\rvert \leq \lvert\varepsilon_0\rvert$
CP	Fracture of more than 50% of boundary bars or horizontal bars	$D \leq D_{cr}$ (for 50% of boundary/horizontal bars)
	Severe confined concrete crushing	$\lvert\varepsilon_{c,vert}\rvert \leq \lvert\varepsilon_{cf}\rvert$
	Severe web concrete crushing	$\lvert\varepsilon_{c,diag}\rvert \leq \lvert\varepsilon_u\rvert$

strain of ε_0, which—based on Figure 4A—is the strain corresponding to onset of compressive strength degradation for unconfined concrete. Thus, to ensure that a wall remains in the IO performance level, the tensile strain of the steel material in the vertical elements must not exceed 1%, while the magnitude of the compressive strain in the concrete material of the vertical elements must not exceed $|\varepsilon_0|$.

An additional type of damage that must be considered is inclined (shear) cracks, which may occur even for flexure-dominated walls. Descriptions in the FEMA 306 document[22] indicate that a wall may have stiffness degradation when the width of inclined cracks exceeds a value of 1/16 inches (1.6 mm). For a simulation using truss models, crack width can be associated to the tensile strain in the inclined truss elements. Neglecting the elastic part of the strain in a cracked element, a crack width w_{cr} must equal the product $\varepsilon_d \bullet L_d$, where ε_d is the axial strain and L_d is the length of the truss element. Based on this rationale, to ensure an IO performance level, the tensile strain in the inclined truss elements of a model must not exceed the value w_{cr}/L_d, where w_{cr} is equal to 1.6 mm.

The acceptance criteria for the IO state are summarized in Table 5. To satisfy this performance level, all three strain conditions corresponding to vertical steel, boundary vertical elements and diagonal elements need to be met, that is, exceedance of one condition implies exceedance of the performance level.

5.2 | Life Safety (LS) level

According to ASCE/SEI 41-17, the LS level corresponds to a state in which the structure exhibits damage but still has a margin of safety against collapse. The limit values of acceptable deformations for LS in this standard typically correspond to the instant right before the lateral strength degradation is initiated. For flexure-dominated components, strain limits proposed in previous studies for LS[6,8] have included steel strains at the onset of bar buckling and rupture, or crushing of confined concrete.

The initiation of strength degradation in flexure-dominated walls is typically associated with the first occurrence of rupture in the reinforcing steel or with the onset of compression-induced failure in the boundary regions of the section. Compressive failure is expected to involve crushing of the confined core concrete and buckling of the vertical reinforcement.[23,38,41,42,43] For shear-dominated strength degradation, a distinction is made between diagonal tension and diagonal compression failures. The former involves the formation of large, localized inclined cracks, and strength degradation is expected to be initiated due to rupture of the horizontal reinforcement crossing these cracks. The latter is associated with diagonal crushing failure in the web concrete, which corresponds to compressive strength degradation in the inclined truss elements of a truss model.

Based on the above considerations, to ensure that a wall satisfies the LS performance state conditions, the conditions presented in Table 5 must be met. Specifically, there must be no rupture in any vertical or horizontal reinforcing bar. In the analyses considered herein, this criterion implies that the internal variable D at each reinforcing steel bar must be less than the threshold value D_{cr} corresponding to bar rupture. Second, the magnitude of the vertical strain of confined concrete must not exceed the value $0.75|\varepsilon_{cf}|$, where ε_{cf} is the strain corresponding to the failure of concrete core, as described in a previous section. This limit has been established below ε_{cf} to provide some margin against this type of failure, which is deemed very brittle based on the experimental evidence. Finally, to ensure that web crushing has not occurred, the magnitude of the compressive strain in the concrete material of the inclined truss elements must not exceed the value $|\varepsilon_0|$.

TABLE 6 Determination of ASCE/SEI 41-17 backbone curve

Wall ID	V_n (kN)	V_y (kN)	V_u (kN)	Control behavior	*IO*(drift ratio)	*LS*(drift ratio)	*CP*(drift ratio)
Wall #1	727	522	571	Flexural	0.58%	1.40%	1.81%
Wall #2	680	404	459	Flexural	0.61%	1.54%	2.00%
Wall #3	1708	479	545	Flexural	0.62%*	1.50%*	1.94%*
Wall #4	468	416	469	Flexural	0.61%	1.41%	1.86%
Wall #5	524	472	585	Shear	0.40%	1.50%	2.00%
Wall #6	602	731	865	Shear	0.40%	0.75%	1.00%

*Plastic hinge rotation.

5.3 | Collapse prevention (CP) level

The ASCE/SEI 41-17 standard defines CP as a state for which the structure is still capable of carrying gravity loads but has no margin of safety against collapse. In other words, the deformations at the CP limit state are those corresponding to the onset of collapse. The envelope curves provided in the standard entail a significant drop in the capacity at the deformations corresponding to the CP limit.

Major strength degradation is expected to occur if a significant portion of the reinforcing bars rupture, a boundary element crushes due to rupture of confining steel, or the diagonal compressive struts forming in the web of a wall have undergone complete degradation of their strength. For the latter, complete compressive strength degradation for the unconfined concrete struts is obtained whenever the material reaches compressive strains equal to ε_u, as shown in Figure 4A. In accordance with these considerations, a wall is assumed to satisfy the CP performance requirements, when less than half of the vertical bars in the boundary and less than half of the horizontal bars in the web have undergone fracture. Additionally, the magnitude of the strain of the boundary vertical elements must not exceed the value $|\varepsilon_{cf}|$, and the magnitude of concrete compressive strain at all inclined truss elements in the web must not exceed the value $|\varepsilon_u|$. The acceptance criteria for the CP state are summarized in Table 5.

6 | PERFORMANCE ASSESSMENT OF WALL COMPONENTS

This section presents a performance assessment of the six wall specimens considered in the analytical study, using the strain-based criteria proposed in the previous section. The procedure employed involves the determination of the points on the analytically obtained load-deformation curves corresponding to the acceptance limits for IO, LS, and CP performance states, as shown in Figure 9. The same figure presents backbone load-deformation curves and limit points determined using the nonlinear modeling and acceptance parameters of ASCE/SEI 41-17.

Important information for establishing the ASCE/SEI 41-17 curves of the walls is summarized in Table 6. The governing response mode of each wall (flexural or shear) needs to be known before the determination of the ASCE/SEI 41-17 curve. For flexure-dominated walls, the lateral force V_y and V_u correspond to the ordinates of points B and C of the curve shown in Figure 1A. The value of V_y is obtained by calculating the nominal flexural strength of the wall section using expected material properties, while V_u is obtained from the maximum inelastic flexural strength, which is calculated by increasing the expected yield strength of steel by 25% to account for strain hardening effects. If the nominal shear strength of a RC wall (V_n) is less than the shear demand corresponding to the nominal flexural strength (V_y), the wall is regarded as shear-dominated. In this case, the load-versus-deformation curve has the shape of Figure 1B. The acceptable drift ratio values per ASCE/SEI 41-17 for each performance state are determined based on the reinforcement configuration, shear demand, and axial loading condition of the wall, in accordance with ASCE/SEI 41-17. For flexure-dominated walls, the ASCE/SEI 41-17 curve uses plastic hinge rotation as the deformation. For Wall #3, the results are directly compared in terms of lateral force versus hinge rotation. For the rest of the walls classified as flexure-dominated in Table 6, the ASCE 41-17 hinge rotation values are converted to drift ratios based on the assumption that the plastic hinge length is equal to 50% of the wall length. Given the lack of more specific guidelines, the deformation value at point D in the backbone curves has been taken equal to that of point C for flexure-controlled walls. For shear-controlled walls, the drift value at point D is determined in accordance with Epackachi et al[3] but it is not taken larger than point E defined in ASCE/SEI 41-17.

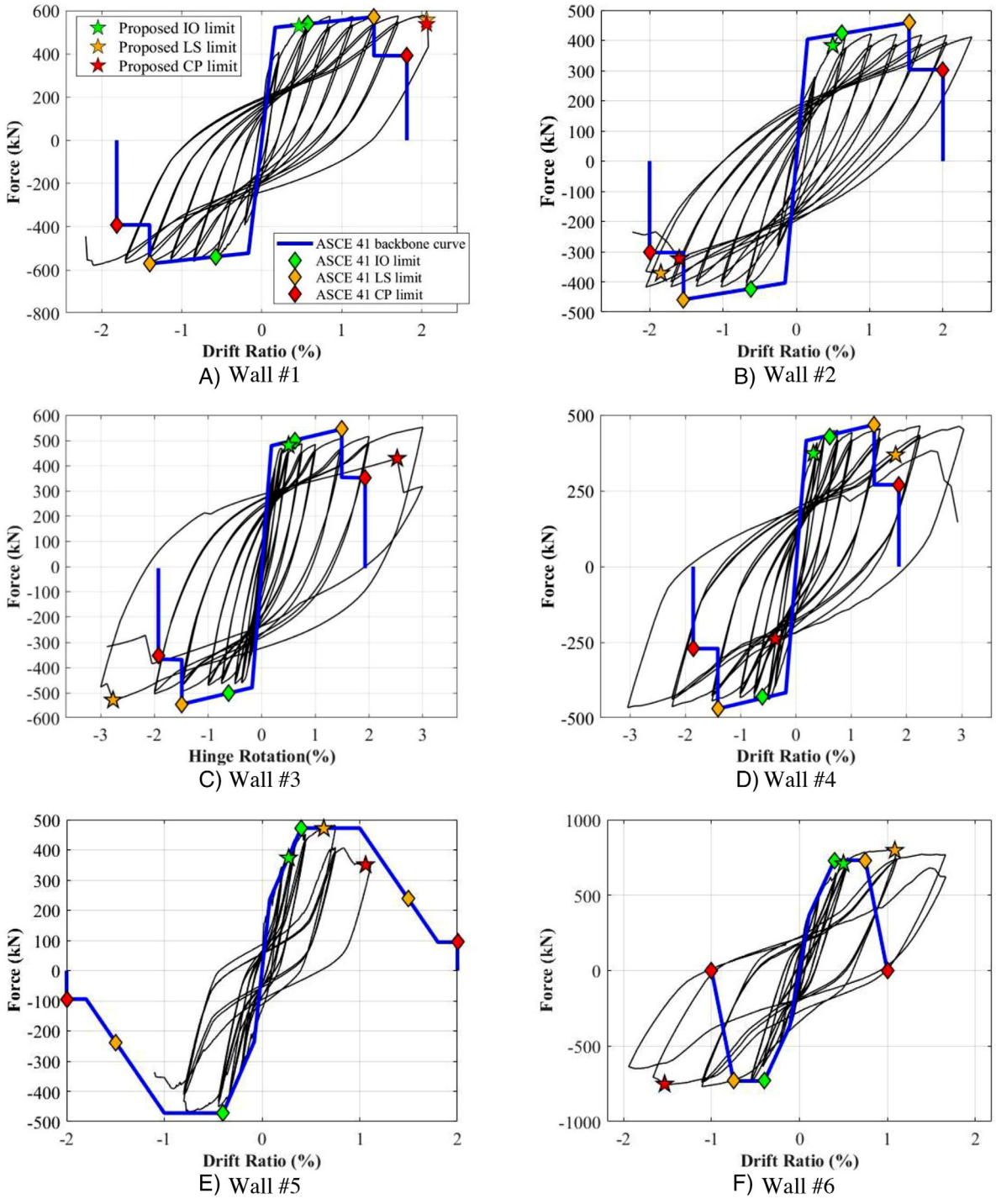

FIGURE 9 Comparison of proposed acceptance criteria and ASCE/SEI 41-17 backbone curve and acceptance limits

The strain-based assessment method predicts that the IO limit in all walls except Wall #5 is determined by concrete spalling ($|\varepsilon_{c,vert}| = |\varepsilon_0|$). For Wall #5, the IO limit is associated with the inclined crack width ($\varepsilon_{c,diag} = w_{cr}/L_d$). While yielding of bars generally occurs prior to the IO limit, the 1% strain limit for steel does not control exceedance of this performance level in any of the cases considered. Based on the data presented in Figure 9, exceedance of IO occurs near the instant beyond which the lateral strength value does not significantly increase with further deformations and the system begins developing irreversible deformations, which is consistent with the occurrence of permanent damage. Exceedance of LS for Wall #2 and Wall #3 is given by the first vertical bar rupture ($D = D_{cr}$) at a drift ratio of 2% and hinge rotation of 3%, respectively. For Wall #4, this limit corresponds to the first horizontal bar rupture ($D = D_{cr}$) during the second loading

cycle at a drift ratio of 2%. The LS limit points in Wall #5 and Wall #6, are determined by the onset of diagonal web crushing ($|\varepsilon_{c,diag}| = |\varepsilon_0|$). As shown in Figure 9, small drops in the lateral load resistance are generally observed after the LS limits, which is consistent with the onset of strength degradation associated to the exceedance of this performance level. For Wall #1, LS exceedance is controlled by the vertical strain at the boundary element ($|\varepsilon_{c,vert}| = 0.75|\varepsilon_{cf}|$) and it coincides in the same analysis increment with the CP limit point ($|\varepsilon_{c,vert}| = |\varepsilon_{cf}|$) due to fast progression of concrete crushing of the confined boundary element, which is consistent with the brittle nature of the specific failure mode. For Wall #2 and Wall #3, the CP limit points correspond to the rupture of 50% of the bars in one of the boundary zones, while Wall #4 attains this limit when 50% of the horizontal bars incur rupture during the first cycle for a drift ratio of 3%. In these three walls, this limit is attained one cycle after LS is exceeded, and after having achieved the same or slightly higher wall deformation amplitude. Both Wall #5 and Wall #6 have CP limit points determined by diagonal crushing of the web.

For the majority of the walls considered, the proposed strain-based acceptance criteria are found to provide a slightly earlier prediction of IO exceedance as compared to the predictions based on the ASCE/SEI 41 criteria. This can be attributed to the fact that ASCE/SEI 41-17 allows some degree of inelasticity at the component level for IO. The LS and CP performance levels given by the proposed strain-based criteria are generally allowing similar levels of deformation capacity as ASCE/SEI 41-17 for Wall #1 and Wall #2. However, ASCE/SEI 41-17 curves are not predicting the correct damage level for the other walls considered. Specifically, the backbone curve obtained based on ASCE/SEI 41-17 underestimates the deformation capacity of Wall #3 and Wall #4. The latter exhibited a diagonal tension failure, despite being classified as flexure-controlled. The deformation capacities of Wall #5 and Wall #6, both classified as shear-controlled based on ASCE/SEI 41-17, are overestimated and underestimated, respectively.

7 | DISCUSSION

The enhanced truss-based modeling scheme used in the present study is capable of capturing the hysteretic response and damage patterns for all common failure modes of planar walls. This fact means that the method could be used in an evaluation based on ASCE 41-17 to derive alternative modeling parameters and acceptance criteria following a similar peer-review procedure as that allowed in Section 7.6 of this standard for experimental data. The proposed strain-based acceptance criteria are expected to have generic applicability for truss models, as the damage mechanisms and material local quantities used to describe them are generally valid. Still, it is acknowledged that the specific values proposed for several of the criteria constitute an initial calibration, which partially relies on prior performance-based design and assessment guidelines and has been verified with a limited set of experimental tests. Future refinements of these limits with a more extensive set of data from experimentally tested walls are necessary to increase the level of confidence and extent of validity.

The proposed assessment method relies on the ability of the truss models to predict the local damage mechanisms, which are quantified through strains in steel and concrete. For this reason, it is interesting to compare the experimentally recorded and analytically obtained strains for the wall tests for which recorded strain data was available. In specific, Table 7 provides a comparison of vertical strains of the boundary reinforcement or boundary element near the wall base, obtained at the peak displacement of different loading cycles for several tests. The analytical and experimental values are in general in good agreement, even though the models tend to underestimate compressive strains for large drift levels. The latter can be attributed to the spurious increase of compressive strength and stiffness resulting from the overlap of inclined and vertical elements in the boundary regions of the truss models, as previously described. For Wall #5, there is also a discrepancy between analytical and experimental tensile strains, but the specific wall was dominated by diagonal tensile cracking. To verify the local demands for this dominant damage mode, a comparison for the diagonal crack width values of Wall #5 has also been conducted. At a drift ratio of 0.44%, the diagonal crack widths measured in the test ranged from 1.3 to 2.4 mm, while the analytically obtained crack widths (calculated as the product of the tensile strains in the diagonal truss elements multiplied by the length of these elements) ranged between 1.4 and 2.7 mm. At the instant where the structure reached its maximum lateral resistance, the experimentally measured diagonal crack widths ranged between 1.3 and 5.5 mm, and the corresponding analytical quantities ranged between 2.3 and 5.6 mm.

The above comparisons indicate an overall reasonable agreement between the analytical predictions and the experimentally recorded strains and crack widths. This is expected since the models are able to capture the dominant damage mode, onset of strength degradation, and actual material failure mechanism leading to strength degradation of the test specimens. Nevertheless, it is important to mention that a direct comparison of local strains obtained in a physical test and a model with phenomenological material laws may not be fully meaningful. While phenomenological material models may be capable of providing good global response quantities, they should not be expected to fully match the local

TABLE 7 Comparison of experimental and analytical vertical strains

Wall #1	**Element**	**Cycle ID**	**9**	**16**	**26**	**36**	**46**	**59**
	Steel in tension	Experiment	0.0012	0.0044	0.0097	0.0154	0.0208	0.0247
		Analysis	0.0013	0.0034	0.0100	0.0128	0.0148	0.0217
	Steel in compression	Experiment	−0.0009	−0.0029	−0.0049	−0.0074	−0.0108	−0.0135
		Analysis	−0.0011	−0.0026	−0.0037	−0.0049	−0.0059	−0.0066
Wall #2	**Element**	**Cycle ID**	**9**	**16**	**26**	**36**	**46**	**59**
	Steel in tension	Experiment	0.0020	0.0053	0.0108	0.0170	0.0228	0.0263
		Analysis	0.0018	0.0044	0.0102	0.0140	0.0178	0.0239
	Steel in compression	Experiment	−0.0008	−0.0018	−0.0034	−0.0053	−0.0063	−0.0055
		Analysis	−0.0013	−0.0031	−0.0034	−0.0049	−0.0037	−0.0031
Wall #3	**Element**	**Cycle ID**	**$\theta = 1.5\%$**	**$\theta = -1.5\%$**	**$\theta = 2\%$**	**$\theta = -2\%$**	**$\theta = 3\%$**	**$\theta = -3\%$**
	Boundary in tension	Experiment	0.0229	0.0252	0.0301	0.0353	0.0458	0.0427
		Analysis	0.0188	0.0181	0.0250	0.0237	0.0414	0.0339
	Boundary in compression	Experiment	−0.0053	−0.0043	−0.0062	−0.0051	−0.101	−0.007
		Analysis	−0.0018	−0.0022	−0.002	−0.0027	−0.0026	−0.0043
Wall #5	**Element**	**Cycle ID**	**4**	**41**	**73**	**124**	**168**	
	Steel in tension	Experiment	0.0014	0.0020	0.0026	0.0076	0.0080	
		Analysis	0.0019	0.0032	0.0061	0.0152	0.0166	
Wall #6	**Element**	**Cycle ID**	**16**	**22**	**25**			
	Steel in tension	Experiment	0.0022	0.0114	0.0162			
		Analysis	0.0029	0.0136	0.0161			
	Steel in compression	Experiment	−0.0021	−0.0062	−0.0066			
		Analysis	−0.0023	−0.0014	−0.0011			

Note: Processed vertical strains were not reported for Wall #4.

stress-strain response at each material point of a physical system. For example, the steel strains in a physical specimen are affected by the concrete tensile strength, the local bond-slip behavior and strain penetration of bars, the actual stress-strain behavior of each bar, and (if applicable) degree of bar buckling. All these quantities are characterized by inherent variability, which is not accounted for in the computational models. In addition, the gage length and positions of the instruments used in the tests and the elements in the truss models do not exactly coincide.

The material damage mechanisms (concrete crushing, bar rupture, etc) considered in the alternative, strain-based acceptance criteria apply to all modeling approaches; hence, the qualitative definition of damage thresholds for a given performance level provided in the second column of Table 5 is general. However, the specific strain quantities corresponding to each damage state will depend on the adopted modeling scheme and constitutive laws. For this reason, the alternative acceptance criteria that have been presented are specific to the truss modeling approach and constitutive laws adopted herein. Other nonlinear analysis schemes, such as continuum finite element models, may require different acceptance criteria. Of course, a first step before formulating acceptance criteria for other simulation approaches is to validate the capability of these approaches to capture all common failure modes for the structural component of interest. To the authors' knowledge, there has not been any other method to date with a demonstrated capability to capture all the failure modes considered here.

A point worth mentioning is the potential applicability of the modeling approach and performance metrics to cases involving three-dimensional effects, such as out-of-plane web buckling or analysis of nonplanar walls. While such cases are outside the scope of the present study, the shell macroelements in the implementation of the truss modeling approach have the capability to account for out-of-plane (flexural) resistance of planar wall elements, in accordance with the beam-truss-model.[19] Geometric nonlinearity has also been incorporated in the models, allowing to naturally account for the impact of, for example, out-of-plane buckling of thin planar elements. The capability of the BTM to capture the hysteretic response and failure of nonplanar walls and wall components undergoing inelastic out-of-plane buckling has been previously validated.[17–21] A recent report[44] has demonstrated the capability of the implementation in *FE-MultiPhys* to successfully simulate these same cases. Given that strength degradation and failure even for the aforementioned cases

is ultimately driven by damage in the material (eg, compressive crushing in the concrete), it is reasonable to expect that the strain-based acceptance criteria formulated herein for planar walls will be valid for cases involving three-dimensional effects. Still, it is acknowledged that further research is necessary to determine whether there are additional local damage mechanisms to be accounted for in cases involving three-dimensional effects, or the impact of such effects on the calibrated values associated with the acceptance criteria.

Two failure modes that can occur for existing RC walls and have not been considered in this study are associated with horizontal shear-sliding and lap-splice slip. Earlier work focused on fully grouted reinforced masonry walls[45,46] found that truss models were able to capture shear-sliding failures. Further work, which is outside the scope of this paper, is necessary to validate the generic applicability of truss models to the analysis of shear-sliding failures in RC walls and to develop pertinent performance acceptance criteria for new failure modes. An advantage of the alternative performance evaluation methodology proposed herein, is that any additional performance acceptance criteria related to, for example, shear-sliding damage or lap-splice failures, can be appended to the criteria listed in Table 5, without any need to modify the latter.

8 | CONCLUSIONS

This paper has proposed a computational simulation scheme to be used for the seismic performance assessment of planar RC walls. The simulation scheme relies on an enhanced implementation of the nonlinear truss modeling approach for RC, which eliminates the need to manually define a line-element assemblage for a wall and has the capability to account for all significant forms of material damage, such as bar buckling and rupture, compressive crushing of concrete, and diagonal concrete degradation. The proposed analysis scheme has been found capable of capturing all possible damage modes which ultimately lead to flexural, diagonal tension and diagonal compression failures at the component level.

Using the conceptual definitions of the immediate occupancy (IO), life safety (LS), and collapse prevention (CP) performance levels in ASCE/SEI 41-17, acceptance criteria for the three levels have been established based on maximum strain values or strain-related parameters for concrete and reinforcing steel obtained from the truss models. Given that the response at the material level is independent of the wall geometry and loads, the specific criteria are expected to demonstrate satisfactory predictive capability for evaluation of RC wall structures presenting a variety of configurations and loading conditions. The analytically obtained lateral deformation curves and drift (or hinge rotation) values at which the acceptance criteria are exceeded have been compared with the monotonic evaluation curves obtained based on the ASCE/SEI 41-17 standard. The procedure based on ASCE/SEI 41-17 is found to give accurate representation of the wall behavior and damage states for certain flexure-dominated walls, but it may not be accurate in predicting the deformability for walls exhibiting a combined flexure-shear inelastic deformation mode.

The proposed computational scheme and performance limits can be used to provide envelope and cyclic hysteretic curves and to calibrate acceptance criteria for use in seismic evaluation, in accordance with the peer-review process described in ASCE 41-17. This approach can contribute to the more accurate seismic assessment of existing RC wall buildings and result in more efficient retrofit design for walls exhibiting mixed flexure-shear failure modes. Still, the limit values used for the various strain-based acceptance criteria have been validated using a fairly limited set of data from experimental tests. For this reason, a more extensive set of experimental data may be necessary for further verifying and—if necessary—fine-tuning the values associated with each limit state. While the damage states considered herein are valid for other types of modeling approaches, such as continuum finite element models, the presented strain-based criteria are specific to the modeling approach and constitutive laws adopted in this paper. Before formulating and calibrating strain-based criteria for other analytical approaches, it will be necessary to validate the capability of these approaches to capture all important failure modes of planar RC walls.

ACKNOWLEDGMENTS

The research presented in this paper is supported by the National Institute of Standards and Technology (NIST) under award No. 70NANB19H060. Any opinions and findings presented in this paper are those of the authors alone, and do not necessarily reflect the opinions of the sponsor.

ORCID

Ioannis Koutromanos https://orcid.org/0000-0002-3556-4258
Juan Murcia-Delso https://orcid.org/0000-0001-6424-7262

REFERENCES

1. ASCE. *Seismic Rehabilitation of Existing Buildings*, ASCE/SEI 41-17. Reston, VA, United States: American Society of Civil Engineers; 2017.
2. Elwood KJ, Matamoros AB, Wallace JW, et al. Update to ASCE/SEI 41 concrete provisions. *Earthquake Spectra*. 2007;23(3):493-523.
3. Epackachi S, Sharma N, Whittaker A, Hamburger RO, Hortacsu A. A cyclic backbone curve for shear-critical reinforced concrete walls. *ASCE J Struct Eng*. 2019;145(4):04019006. 1-14.
4. Kowalsky MJ, Priestley MJN, MacRae GA. Displacement-based design of RC bridge columns in seismic regions. *Earthquake Eng Struct Dyn*. 1995;24:1623-1643.
5. Priestley MJN, Calvi GM. Concepts and procedures for direct displacement-based design and assessment. *Seismic Design Methodologies for the Next Generation of Codes*. New York NY: Taylor & Francis; 1997:171-181.
6. Priestley MJN, Calvi GM, Kowalsky MJ. *Displacement-Based Seismic Design of Structures*. Pavia, Italy: IUSS Press; 2007.
7. Kowalsky MJ, Recent developments on the performance-based seismic design of bridges. *2019 EERI Annual Meeting* , Vancouver, BC, Canada; 2019.
8. Panagiotou M, Restrepo J. Displacement-based method of analysis for regular reinforced-concrete wall buildings: application to a full-scale 7-story building slice tested at UC–San Diego. *ASCE J Struct Eng*. 2011;137(6):677-690.
9. Humar J, Fazileh F, Ghorbanie-Asl M, Pina FE. Displacement-based seismic design of regular reinforced concrete shear wall buildings. *Can J Civ Eng*. 2011;38:616-626.
10. Pugh JS, Lowes LN, Lehman DE. Nonlinear line-element modeling of flexural reinforced concrete walls. *Eng Struct*. 2015;104:174-192.
11. Martinelli L. Modeling shear–flexure interaction in reinforced concrete elements subject to cyclic lateral loading. *ACI Struct J*. 2008;105(6):675-684.
12. Palermo D, Vecchio FJ. Simulation of cyclically loaded concrete structures based on the finite-element method. *ASCE J Struct Eng*. 2007;133(5):728-738.
13. Massone LM, Orakcal K, Wallace JW. Modeling of squat structural walls controlled by shear. *ACI Struct J*. 2009;106(5):646-655.
14. Kolozvari K, Orakcal K, Wallace JW. Modeling of cyclic shear-flexure interaction in reinforced concrete structural walls. I: theory. *ASCE J Struct Eng*. 2015;141(5):04014135. 1-10.
15. Mazars J, Kotronis P, Davenne L. A new modeling strategy for the behavior of shear walls under dynamic loading. *Earthquake Eng Struct Dyn*. 2002;31(4):937-954.
16. Panagiotou M, Restrepo J, Shoettler M, Kim G. Nonlinear cyclic truss model for reinforced concrete walls. *ACI Struct J*. 2012;109(2):205-214.
17. Lu Y, Panagiotou M, Koutromanos I. Three-dimensional beam-truss model for reinforced concrete walls and slabs—part 1: modeling approach, validation, and parametric study for individual reinforced concrete walls. *Earthquake Eng Struct Dyn*. 2016;45(9):1495-1513.
18. Lu Y, Panagiotou M. Three-dimensional beam–truss model for reinforced concrete walls and slabs—part 2: modeling approach and validation for slabs and coupled walls. *Earthquake Eng Struct Dyn*. 2016;45(11):1707-1724.
19. Alvarez R, Restrepo JI, Panagiotou M. RC wall plastic hinge out-of-plane buckling: analysis using the nonlinear beam-truss model. *ASCE J Struct Eng*. 2020;146(12):04020274.1–20.
20. Alvarez R, Restrepo JI, Panagiotou M, Santhakumar AR. Nonlinear cyclic truss model for analysis of reinforced concrete coupled structural walls. *Bull Earthquake Eng*. 2019;17(12):6419-6436.
21. Alvarez R, Restrepo JI, Panagiotou M, Godinez S. Analysis of reinforced concrete coupled structural walls via the beam-truss model. *Eng Struct*. 2020;220:111005.
22. FEMA. *Evaluation of earthquake-damaged concrete and masonry wall buildings: basic procedures manual*, FEMA 306. Prepared by the Applied Technology Council for the Federal Emergency Management Agency, Washington, DC, United States; 1998.
23. Dazio A, Beyer K, Bachmann H. Quasi-static cyclic tests and plastic hinge analysis of RC structural walls. *Eng Struct*. 2009;31(7):1556-1571.
24. Lu Y, Panagiotou M, Koutromanos I. *Three-Dimensional Beam-Truss Model for Reinforced-Concrete Walls and Slabs Subjected to Cyclic Static or Dynamic Loading*. Berkeley, CA: Pacific Earthquake Engineering Research Center; 2014. Report No. PEER 2014/18.
25. Beyer K, Dazio A, Priestley MJN. Quasi-static cyclic tests of two U-shaped reinforced concrete walls. *J Earthquake Eng*. 2008;12(7):1023-1053.
26. Koutromanos I, Farhadi M. *FE-MultiPhys: A Finite Element Program for Nonlinear Analysis of Continua and Structures*. Blacksburg, VA: Department of Civil and Environmental Engineering, Virginia Polytechnic Institute and State University; 2018. Report CE/VPI-ST-18/02.
27. Zhang P, Restrepo JI, Conte J, Ou J. Nonlinear finite element modeling and response analysis of the collapsed Alto Rio building in the 2010 Chile Maule earthquake. *Struct Design Tall Build*. 2017;26(16):e1364.
28. Lu Y, Panagiotou M. Three-dimensional cyclic beam-truss model for nonplanar reinforced concrete walls. *ASCE J Struct Eng*. 2014;04013071:1-11.
29. Vecchio F, Collins M. The modified compression-field theory for reinforced concrete elements subjected to shear. *ACI J Proceed*. 1986;83(2):219-231.
30. Kim S, Koutromanos I. Constitutive model for reinforcing steel under cyclic loading. *ASCE J Struct Eng*. 2016;142(12):1-14.
31. Dodd LL, Restrepo-Posada JI. Model for predicting cyclic behaviour of reinforcing steel. *ASCE J Struct Eng*. 1995;121(3):433-445.
32. Moharrami M, Koutromanos I. Finite element analysis of damage and failure of reinforced concrete members under earthquake loading. *Earthquake Eng Struct Dyn*. 2017;46(15):2811-2829.
33. Girgin S, Moharrami M, Koutromanos I. Nonlinear beam-based modeling of RC columns including the effect of reinforcing bar buckling and rupture. *Earthquake Spectra*. 2018;34(3):1289-1309.

34. Dhakal RP, Maekawa K. Path-dependent cyclic stress-strain relationship of reinforcing bars including buckling. *Eng Struct*. 2002;24(11):1383-1396.
35. Mander J, Priestley MJN, Park R. Theoretical stress–strain model for confined concrete. *J Struct Eng*. 1988;114(8):1804-1826.
36. Karthik MM, Mander JB. Stress-block parameters for unconfined and confined concrete based on a unified stress-strain model. *J Struct Eng*. 2011;137(2):270-273.
37. Mander JB. *Seismic design of bridge piers*. Doctoral dissertation, University of Canterbury, Christchurch, New Zealand; 1983.
38. Segura CL, Wallace JW. Seismic performance limitations and detailing of slender reinforced concrete walls. *ACI Struct J*. 2018;115(3):849-860.
39. Tran TA, Wallace JW. Cyclic testing of moderate-aspect-ratio reinforced concrete structural walls. *ACI Struct J*. 2015;112(6):653-666.
40. Mestyanek JM. *The earthquake resistance of reinforced concrete structural walls of limited ductility*. Master of Engineering Thesis, University of Canterbury, Christchurch, New Zealand; 1986.
41. Oesterle R, Aristizabal-Ochoa J, Fiorato A, Russel H, Corley W. *Earthquake Resistant Structural Walls—Tests of Isolated Walls—Phase II*. Skokie, IL: Construction Technology Laboratories, Portland Cement Association; 1979. Report to the National Science Foundation.
42. Villalobos EJF. *Seismic response of structural walls with geometric and reinforcement discontinuities*. PhD thesis, Purdue University, West Lafayette, IN; 2014.
43. El-Azizy OA, Shedid MT, El-Dakhakhni WW, Drysdale RG. Experimental evaluation of the seismic performance of reinforced concrete structural walls with different end configurations. *Eng Struct*. 2015;101:246-263.
44. Panagiotou M, Koutromanos I. *Advanced and practical seismic analysis of reinforced concrete walls and building systems using the BTM-Shell methodology in the program FE-MultiPhys*. Report, School of Earthquake Resilient Design; 2020, DOI: https://doi.org/10.13140/RG.2.2.27772.97924.
45. Moharrami M, Koutromanos I, Williams S. Analysis of shear-dominated reinforced masonry walls using truss models. *Masonry Soc J*. 2015;33(1):27-48.
46. Moharrami M, Koutromanos I, Panagiotou M. Nonlinear truss modeling method for the analysis of shear failures in reinforced concrete and masonry structures. *Proceedings of the Second ATC & SEI Conference on Improving the Seismic Performance of Existing Buildings and Other Structures*, San Francisco, CA; 2015.

How to cite this article: Deng X, Koutromanos I, Murcia-Delso J, Panagiotou M. Nonlinear truss models for strain-based seismic evaluation of planar rc walls. *Earthquake Engng Struct Dyn*. 2021;50:2939–2960. https://doi.org/10.1002/eqe.3480